Novel Dynamics are Represented as a Mixture of Multiple Coordinate Systems

Raz Leib, David W. Franklin

Abbreviated title: Mixed Coordinate System Representation of Dynamics

Affiliation:

Neuromuscular Diagnostics, Dept. of Sport and Health Sciences, Technical University of Munich, 60/62 Georg-Brauchle-Ring 80992 Munich, Germany

Corresponding Author: David W. Franklin (david.franklin@tum.de)

Conflict of Interest: The authors declare no competing financial interests.

Acknowledgments: We thank Christian Stockinger for his contributions to an early version of this experiment.

Abstract

Skillful and accurate object manipulation requires the object's dynamics to be represented within a motor memory. Despite extensive research, how the motor system represents novel dynamics is still an open question. This representation is normally examined by testing the spatial generalization of the learned forces. However, previous studies have not been able to provide a consistent view of this representation in the motor system, with each study providing evidence favoring an extrinsic coordinate system, an intrinsic coordinate system, an object-based representation, or mixtures of these coordinate systems, but no study could definitively exclude other possibilities. Most previous studies used a skew viscous force field, but these force fields limit the use of channel trials and can therefore prevent us from distinguishing between different coordinate systems. Here we propose a novel method to overcome these disadvantages, by developing a new force field in which a curl force field is scaled by a trigonometric function of movement direction allowing precise assessment of the learned generalization. In a series of four experiments we show that the representation of ambiguous external dynamics is formed by a mixture of extrinsic, intrinsic and object-based coordinate systems with a slightly higher weighting for the object-based representation compared with Cartesian or joint representations. These results highlight the existence of multiple representations in the motor system but more importantly it shows that for certain dynamics the motor system prefers representation using a mixture of representations over single frame based representation.

Introduction

During object manipulation, such as swinging a jump rope, we experience external forces. To manipulate the object, we need to estimate the mapping between the motion and the resulting forces, and then send appropriate commands to the muscles that compensate for the arm and object dynamics. While this seems trivial, it is still unknown how we represent the dynamic mapping of such tasks, as there are at least three different reference frames that can solve this problem. First, we could use a Cartesian coordinate frame in which the forces are represented as vectors in a coordinate system located externally to the body. Second, we could represent the forces using the shoulder, elbow and wrist joint torques. Third, we could calculate the forces using the orientation vector connecting between the shoulder and the object or hand in space (Berniker et al., 2014).

One way to distinguish between these representations is by examining how dynamics are generalized in space. In dynamic generalization, participants learn to move under force perturbations (Shadmehr and Mussa-Ivaldi, 1994) followed by testing how the learned dynamics are extrapolated to new locations in space. Although many studies have used dynamic generalization to address the topic of representation, the results do not provide a consistent view of the coordinate frame used by the motor system. Some studies support a Cartesian based representation (Criscimagna-Hemminger et al., 2003), while others support a joint-based (Shadmehr and Mussa-Ivaldi, 1994) or object-based representation (Yeo et al., 2015; Franklin et al., 2016). In addition, some studies suggested that the system uses a mixture of the aforementioned coordinate frames (Parmar et al., 2011; Berniker et al., 2014). However, even in these studies a range of possible coordinate frames could explain the data. For example, although Berniker et al. (2014) suggested that the mixture of coordinate frames described adaptation, they were unable to distinguish between five different models, including both single coordinate frame models, and ones with and without spatial decay. The lack of consistency between these results raises the question as to the true nature of this internal representation.

We suggest that one reason for this inconsistency in results is that most studies used a velocity dependent force field implemented using a skew matrix. That is, for most movement directions, the forces applied on the hand consist of both forces perpendicular to movement direction and (assistive or resistive) forces in the same direction as the movement. In such cases, two major problems complicate detection of generalized forces. First, we are not able to accurately measure

the generalized forces. Usually, to measure these forces we apply a force channel (Scheidt et al., 2001), a virtual force field constraining the hand to move in a straight path to the target. The applied forces on the virtual channel are the forces that the motor system generates to contradict the expected external forces. While this method has great advantages, it cannot detect the forces in the skew force field that are not perpendicular to movement direction. Second, a skew force field will produce assistive or resistive forces in the direction of movement, which can alter the movement kinematics when moving in a force channel (Berniker et al., 2014). This could cause the participant to miss the target, but more importantly could change the spatial or temporal nature of the generalized forces.

To overcome these disadvantages, we used a velocity dependent curl force field, which generates perpendicular forces on the hand, and by scaling differently the forces according to movement direction, forces generated along one motion direction differ in amplitude and sign compared with other directions. Critically, this variation in the forces means that we can examine the directional change of the generalized forces compared with the learned force to distinguish between different representations. Here we show that the representation of ambiguous novel dynamics is formed by a mixture of coordinate frames with a slightly higher weighting for the object-based representation.

Methods

Participants

Thirty-two right-handed participants (14 females; aged between 22-35) participated in one of four experiments after signing a consent form and completing a handedness test (Oldfield, 1971). The experimental protocol was approved by the Ethics Committee of the Medical Faculty of the Technical University of Munich. Each participant only performed one of the four experiments.

Experimental Setup

We created a haptic augmented virtual reality environment using a vBOT robotic device (Howard et al., 2009). The robotic device was used to record hand position and velocity while generating force feedback at 1 kHz in real time. A six-axis force transducer (ATI Nano 25; ATI Industrial Automation) measured the end-point forces applied by the participant on the handle and was also sampled at 1 kHz. Participants were seated in front of the experimental setup and looked at a semi-silvered mirror showing the projection of an LCD screen placed directly above it (Figure 1A) such that visual feedback was presented in the plane of arm movement. An opaque screen below the mirror prevented participants from viewing their hand. The participant grasped the robotic handle using his/her right hand with their arm supported on an air sled allowing frictionless movement. Once the participant was seated in front of the system we measured the shoulder position in system coordinates. To do so, we initially measured the upper arm length and length between elbow joint to the handle center. Next, we placed the hand at the system center location by applying forces using the robot and measured the elbow and shoulder angles. Using these measurements and the inverse kinematics equations of a two-link arm model, we calculated the shoulder location.

Participants performed point-to-point reaching movements between a start position and a target position. The participants saw on the screen a cursor (red circle with diameter of 0.7 cm) representing their hand. Each trial was started by the robotic system moving the participant's hand to the start position (1.5 cm diameter gray circle) in which the participants were instructed to wait for a go cue. After a random wait time varying between 0.75 and 1.5 s, a short auditory beep signaled participants to start their movement towards the target (yellow circle with 1.5 cm diameter). The start and target points were chosen from 16 equally spaced locations on a 10 cm diameter circle (Figure 1B). Participants were instructed to move with a consistent peak speed of

50cm/s. To do so, at the end of each movement participants were presented visual feedback about the peak speed of their movement. Peak speed that was within ±8cm/s from the desired peak speed was considered ‘good’ while a peak speed below this value received a ‘too slow’ message and above it received a ‘too fast’ message. In addition, if the participants overshoot the target position by more than 2cm, they received an ‘overshoot’ message. For each movement that was considered as a good movement, we increased a score that appeared on the top of the screen by one point.

On each trial, the robot was used to produce one of three virtual environments. The first was a null field (NF), in which the robot was completely passive. For the other two environments, the robot generated forces on the participants’ hand during movement. The second virtual environment was a *force channel* (Scheidt et al., 2001; Milner and Franklin, 2005; Smith et al., 2006), on which we implemented two virtual walls that constrained the participants’ hand to move in a straight-line path to the target. The virtual walls were created by generating forces that were perpendicular to the line connecting between the start and target positions. The forces were calculated according to the deviation of the hand position from the straight-line path multiplied by a stiffness coefficient of 4000 N/m and the velocity in the movement perpendicular direction multiplied by a damping coefficient of 2 Ns/m. The third type of virtual environment was a *force field*. During these trials, participants experienced forces acting on their hand that were a function of the hand’s instantaneous velocity. The forces were calculated using a scaled curl matrix

$$\begin{bmatrix} F_x \\ F_y \end{bmatrix} = B(\dot{x},\dot{y}) \cdot \begin{bmatrix} \dot{x} \\ \dot{y} \end{bmatrix} = \begin{bmatrix} 0 & 0.16 \\ -0.16 & 0 \end{bmatrix} \cdot \cos\left(2 \cdot \arctan\left(\frac{\dot{y}}{\dot{x}}\right)\right) \cdot \begin{bmatrix} \dot{x} \\ \dot{y} \end{bmatrix} \qquad [1]$$

where F_x and F_y are the forces generated in the x and y axis respectively and $\dot{x}$ and $\dot{y}$ are the hand velocities in the x and y axis respectively. The traditional curl force field was scaled using a cosine trigonometric function of movement direction. That is, the magnitude and sign of the scaling factor changed according to movement direction, calculated using the inverse tangent function (Figure 1C). For example, when the motion was made only in the x-axis, i.e. horizontal right to left or vice-a-versa, the scaling factor was equal to 1, or when the motion was made only in the y-axis, i.e. moving away or towards the body, the scaling factor was equal to (-1). We define clockwise forces as positive forces and counter-clockwise forces as negative forces. Simulated mean forces that participants experienced can be illustrated as a cosine curve when plotted as a function of movement direction (Figure 1D).

Experimental Protocol

We conducted four experiments using similar experimental protocols. For each experiment, we used three workspaces (differing in their spatial location) in which participants performed the reaching movements; one *training workspace* and two *test workspaces*. Each experiment included four experimental phases (Figure 1E). The experiment started with a familiarization phase of 16 trials that was performed only in the training workspace. In this phase, participants performed reaching movements from each one of sixteen starting points. The movements were unconstrained reaching movements, i.e. there were no forces applied on participants' hand (NF condition). The second, pre-exposure phase included recording baseline measurements of the movements in the force channel. For this purpose, participants performed 384 movements overall in the training and test workspaces. The movements included both unconstrained reaching movements (NF condition) and movements while the robot generated a virtual force channel between start and target locations (FC condition). Participants performed 4 NF and 4 FC trials for each of the sixteen starting points in each workspace, which means that for each workspace participants performed 128 movements (total 384 movements across the three workspaces). During the third, exposure phase, participants experienced the forces generated by the trigonometric-scaled curl force field (FF condition). Participants performed 15 repetitions from each of the 16 starting points (total of 240 trials), all performed in the training workspace. Finally, after adaptation to the force field, the fourth phase tested generalization of the force field representation in the two test workspaces. During this phase, participants performed 1536 reaching movements in the training workspace on which the force field was applied and an additional 384 movements in the training and test workspaces in which their movements were constrained within the force channel. For each workspace, we had 8 repetitions of force channel trials for each of the 16 starting points (total 384 trials). These trials were randomly introduced within the 1536 of force field trials; for every series of 4 force field trials we had one force channel trial. The position of the force channel trial within the series was random with a uniform distribution. Each participant participated in one of four experiments, which differed in the location of the training and test workspaces or had an additional task besides performing reaching movements.

Experiment 1. The location of the center of the training workspace was set for each participant so that the participants' shoulder joint was at 50° and elbow joint was at 90°. The center of the test

workspace 1 was set so with participants' shoulder angle at 50° and elbow angle at 55°. The center of test workspace 2 was set with the shoulder joint at 75° and elbow at 45° (Figure 2A).

Experiment 2. The location of the center of the training workspace was set for each participant so that the participants' shoulder joint was at 40° and elbow joint was at 70°. The center of the test workspace 1 was set so with participants' shoulder angle at 75° and elbow angle at 85°. The center of test workspace 2 was set with the shoulder joint at 75° and elbow at 50° (Figure 2D).

Experiment 3. The location of the training and test workspaces were set specifically for each participant and identical to those of experiment 2. However, in this experiment the participant's hand always moved in the training workspace (both training and test workspaces). Movements in the test workspaces were performed using a virtual pole attached to the participants' hand. That is, a virtual green pole linked the red cursor representing the participants' hand to a green cursor located in the test workspace. This green cursor then moved with this fixed offset to the participant's hand, as the participant's hand moved. We instructed participants to move the green circle between the start and target instead of their hand. The length and orientation of the pole was set based on the vector connecting the center of the training and test workspaces (Figure 2G). In order to move between a particular set of start and target points in the test workspace, participants had to perform similar movement between the same start and target points in the training workspace with their hand. Thus, the joint trajectory was similar regardless of whether it was performed in the training or test workspaces.

Experiment 4. This experiment was similar to experiment 1 or 2 but with different workspace locations (Figure 2J). The center of the training workspace was set for each participant so that their shoulder joint was at 55° and elbow joint was at 75°. The center of test workspace 1 and 2 was set such that the shoulder and elbow joints were oriented at [30°, 100°] and [80°, 50°] respectively. These workspace locations kept the hand orientation constant while the arm configuration varied.

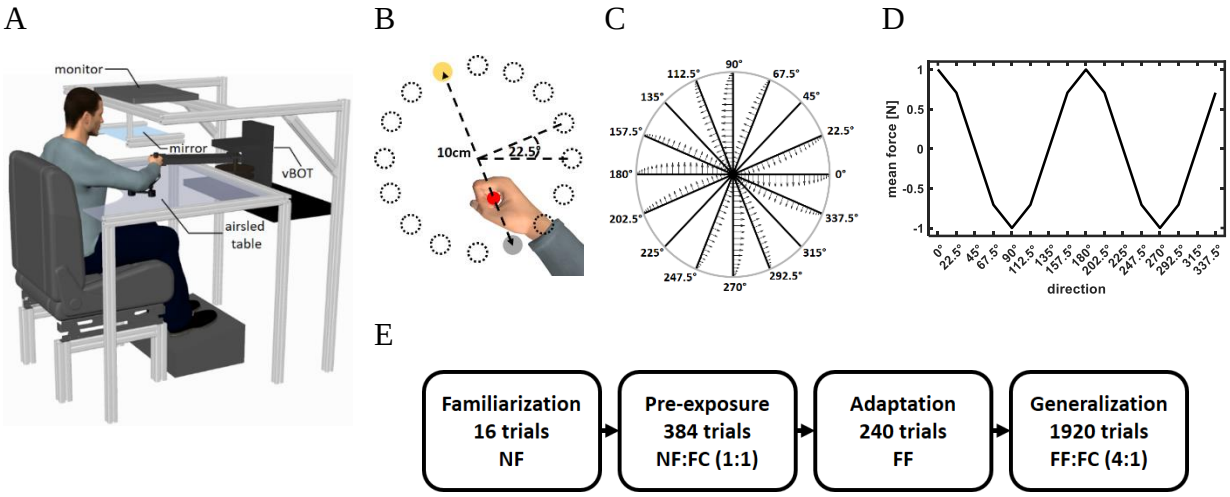

Figure 1: Experimental setup.
A) Participants sat in front of a robotic manipulandum system (vBOT) while grasping the handle of the robot with their right hand. The participants' arm was supported by an airsled system that reduced friction during movement. The virtual environment was projected on a mirror from a monitor mounted above the movement space.
B) Display of the virtual workspace. The participants' hand was represented using a red cursor that was aligned with the hand position. The task was to move from the start point (grey circle) to the target point (yellow circle). The start and target points were always located on the diameter of a 10 cm diameter circle. There were 16 possible starting points spaced evenly on the circumference of the circle. On each trial only one set of start and target points were presented.
C) Endpoint force profiles as a function of movement direction. The forces were calculated using a scaled curl force field (equation 1).
D) Cosine representation of the mean forces of the scaled force field as a function of movement direction. Clockwise forces were set as positive and counterclockwise forces were set as negative.
E) Experimental protocol. Initial familiarization phase included 16 trials in which no force applied on the hand (NF condition). The pre-exposure phase included unconstrained movements (NF condition) and movements in a force channel (FC condition), with a ratio of 1:1 in all three workspaces. In the adaptation phase, participants performed the movements under the force field perturbation (FF condition) only in the training workspace. In the last phase we tested generalization using force channel trials (FC) that were introduced randomly at the training and test workspaces while participants kept moving under force field perturbations (FF) only in the training workspace. The ratio between force field and force channel trials was 4:1.

Data Analysis

Data analysis was performed offline using Mathworks Matlab 2018b®.

Maximum Perpendicular Error (MPE). On each null field or force field trial the maximum distance between the trajectory and the straight line joining the start and target points was calculated as a measure of kinematic error.

Force Compensation. The force compensation was calculated during the generalization phase for the training and test workspaces on the force channel trials. Force compensation in the training workspace indicates the degree of adaptation of individual participants to the force field whereas force compensation in the test workspaces demonstrates how the learned forces are generalized in space. Force compensation was calculated as the regression slope between the perfect force compensation signal, the independent variable, and the recorded force signal, the dependent variable (Smith et al., 2006). The recorded force profile for each channel trial was identified between the start and end of the movement (first and last point at which velocity exceeded 5% maximum velocity). The perfect compensation force profile was determined as the force required for perfect compensation of movement in an unscaled curl force field and was calculated by multiplying the unscaled curl force field matrix by the velocity vector, $\begin{bmatrix} 0 & 0.16 \\ -0.16 & 0 \end{bmatrix} \cdot \begin{bmatrix} \dot{x} \; ; \; \dot{y} \end{bmatrix}$. Here we compare the recorded force profile with forces computed using an unscaled version of the curl force field and not the scaled curl force field for three reasons. First, for some directions there was no force perturbations (e.g. moving at a direction of 45°), even the smallest force participants generate during force channel trials will result in an infinite slope value. The second reason is to capture the direction of the forces that participant generated, i.e. clockwise or counter-clockwise. Regression against always positive values of the perfect force profile allows us to identify in which directions the participants generated positive or negative forces. This allows us to identify any shift in the force compensation profiles when plotted as a function of movement direction. Third, by calculating the regression against the same value across all directions allows us to identify the force magnitude participants adapted to as a function of movement direction. Once we calculated the force compensation measurement for each movement in the force channel, we averaged across the eight repetitions for each movement direction and repeated this for all 16 directions and each workspace. The resulting pattern of the force compensation measure across all movement directions resembles a cosine function. To

quantify phase differences between the scaled force field and the force compensation curves extracted from movements in the training and test workspaces, we calculated the cross-correlation between these cosine signals. That is, the cross-correlation provided a measure for the shift of each force compensation curve from the designed scaled force field.

Prediction of Generalization Models

We considered three different coordinate frames in which the motor system could represent the learned dynamics. By examining the cosine shape of the learned dynamics as a function of movement direction (Figure 1D), we can distinguish in which coordinate system participants represented the forces.

The first coordinate system we considered is the Cartesian coordinate system. For this representation, the forces are invariant with respect to the arm orientation. In such case, participants will exhibit similar forces to the learned forces for each one of the test workspaces (equation 1), resulting in a similar cosine signal of generalized forces as a function of movement direction.

The second coordinate system we considered is the joint-based coordinate system (Shadmehr and Mussa-Ivaldi, 1994; Malfait et al., 2002). For this representation, the generalized forces exhibited in the test workspaces should differ from the learned forces since the arm configuration has changed. That is, for experiment 1, 2, and 4 we expect a change in the cosine function describing the generalized forces. To calculate the expected generalized forces profile, we used a two-link arm model in which $\boldsymbol{\theta} = [\theta_s, \theta_e]$ represents a vector of the shoulder and elbow joints values. Initially, we need to derive the learned dynamics in joint coordinate system and then derive the expected generalized forces. In joint representation, the learned forces are represented as joints torques using the Jacobian which form the relation between the two variables, $\boldsymbol{\tau} = J_{train}^{T} \cdot \boldsymbol{F}$, where $\boldsymbol{F} = [F_x, F_y]$ is a vector of the end-point forces, $\boldsymbol{\tau} = [\tau_s, \tau_e]$ is a vector of joints torques, and J_{train} is the arm's Jacobian matrix for the training configuration. Similarly, the hand velocities are represented using joint angular velocity and the Jacobian matrix, $\boldsymbol{v} = J_{train} \cdot \dot{\boldsymbol{\theta}}$, where $\boldsymbol{v} = [\dot{x}, \dot{y}]$ is the hand velocity vector. Thus, using the end-point forces generated by the force field (equation 1) we derived the learned joint torques

$$\boldsymbol{\tau} = J_{train}^{T} \cdot \boldsymbol{F} = J_{train}^{T} \cdot B(\boldsymbol{v}) \cdot \boldsymbol{v} = J_{train}^{T} \cdot B\left(J_{train} \cdot \dot{\boldsymbol{\theta}}\right) \cdot J_{train} \cdot \dot{\boldsymbol{\theta}} \qquad [2]$$

The expected forces during movement in the test workspaces can be compute using the learned torques and the arm's Jacobian for the test configuration.

$$\begin{aligned} \boldsymbol{F} &= J_{test}^{-T} \cdot \boldsymbol{\tau} \\ &= J_{test}^{-T} \cdot J_{train}^{T} \cdot B\left(J_{train} \cdot \dot{\boldsymbol{\theta}}\right) \cdot J_{train} \cdot \dot{\boldsymbol{\theta}} \\ &= J_{test}^{-T} \cdot J_{train}^{T} \cdot B\left(J_{train} \cdot J_{test}^{-1} \cdot \boldsymbol{v}\right) \cdot J_{train} \cdot J_{test}^{-1} \cdot \boldsymbol{v} \end{aligned} \qquad [3]$$

The third coordinate system we considered is the object-based coordinate system (Berniker et al., 2014). For this representation, the motor system relates the dynamics to a grasped object. When moving outside of the training workspace, the expected forces are calculated according to the orientation of the held object, which is rotated with the hand orientation. For example, if we learned a force profile while moving straight away from the body and we now moved to another location in which the hand was rotated by an angle θ in external space, the learned profile is expected to appear at a direction which is rotated by θ. That is, initially, based on the velocity vector, we can find the learned force profile by rotating back to the original training workspace $\boldsymbol{F}_{train} = B\left(R^{-1}(\theta) \cdot \boldsymbol{v}\right) \cdot R^{-1}(\theta) \cdot \boldsymbol{v}$, where R is a rotation matrix. Then, we rotate these forces to the test workspace:

$$\boldsymbol{F}_{test} = R(\theta) \cdot \boldsymbol{F}_{train} \qquad [4]$$

The predictions of these models for each of four experiments are depicted in Figure 2. We simulated the expected forces according to the models for the two test workspaces using the different arm postures. For experiment 1 (Figure 2B and 2C), using a Cartesian based representation, the expected forces do not change when switching between workspaces. Thus, the force compensation profile is similar to the profile of the force field for both test workspaces 1 and 2. In the case of a joint-based representation, since the arm posture changes between workspaces, the force compensation profile for the test workspace changes compared with the learned force field. For test workspace 1, there is a leftward shift of the force compensation curve compared with the learned force field curve for some of the directions. For test workspace 2 there is a leftward shift for some parts of the signal and a rightward shift for the rest of the signal compared with the learned force field. Similar to the joint-based representation, for object-based representation, the force compensation profiles change as the orientation of the hand is changed between workspaces.

For both workspaces, the curves are shifted to the left with an increased leftward shift for test workspace 1. Thus, leftward shift of the force compensation curve for the test workspace 1 compared to the learned forces curve would suggest that the representation does not rely on a Cartesian based coordinate system. Similarly, leftward shift of the curve for test workspace 2 would suggest that the representation relies more on an object-based representation while a rightward shift would suggest that the representation relies more on a joint-based representation.

For experiment 2 (Figures 2E and 2F), the Cartesian based representation again predicts that the expected force profile in the test workspaces will be the same as the adapted force profile in the training workspace. In the case of a joint-based representation or an object-based representation, both predict a shift to the right with an increased rightward shift for test workspace 1.

For experiment 3 (Figures 2H and 2I), both the Cartesian based and joint-based representations predict that the force compensation curves do not change or shift compared with the learned force field curve since the hand posture does not change between the training workspace and test workspaces. However, for the object-based representation, since the orientation of the pole is different between the training and test workspaces, the predictions of the force compensation curve are shifted to the right, more strongly so for test workspace 1. Thus, for this experiment, a rightward shift of the force compensation curves would suggest that representation relies more on an object-based representation.

For experiment 4 (Figures 2J and 2K), the Cartesian based representation again predicts that the expected force profile in the test workspaces will be the same as the adapted force profile in the training workspace. Similarly, the object-based representation predicts the same expected force profile as hand orientation does not change between the training and test workspaces. However, since the arm configuration changes between these workspaces, the joint-based representation predicts alterations in the expected force profiles. For test workspace 1, joint-based representation predicts a shift to the left of the curve for some movement directions while for test workspaces 2 the prediction is a rightward shift of the curve. If instead there are small or no shifts of the curves then this would argue against a joint-based representation.

Alongside the individual model predictions we also considered that representation might be based on a mixture of models (Berniker et al., 2014). That is, we considered that the expected forces in

the test workspaces are calculated as a weighted sum of the expected force values of the individual models:

$$\boldsymbol{F} = k_c \cdot \boldsymbol{F}_{Cartesian} + k_j \cdot \boldsymbol{F}_{joints} + k_o \cdot \boldsymbol{F}_{object} \,. \qquad [5]$$

For this model, we searched for the optimal weights, k_c, k_j, k_o, such that the squared error between the mean force profile of participants and the weighted predicted force, calculated using the simulations, is minimized. For this optimization problem, we constrained the weights to positive values and set the sum of the weights equal to one. The constraint on the weighted sum is a result of assuming that the expected forces in the test workspaces will have the same magnitude as in the training workspace. However, previous studies suggested that the magnitude of the generalized forces might decay as we are moving away from the training workspace (Gandolfo et al., 1996; Berniker et al., 2014). Thus, we also considered a mixture model with a decay factor by constraining the sum of weights to be equal or less than one.

Overall, we considered 14 models; 6 individual models with or without decay, and 8 mixture models covering all combinations of the individual models with and without decay. To compare the performance of the models in explaining the mean generalized force profiles, we used the Bayesian information criterion (BIC):

$$BIC = -2 \cdot \log\left(L\right) + k \cdot \log\left(n\right) \qquad [6]$$

where log(L) is the logarithm of the model likelihood, k is the number of degrees of the model (1 for individual models and 2 or 3 for mixture models), and n=32 is the total number of data points. We fitted the models separately for the results of each experiment and afterwards calculated the BIC for each model where smaller BIC value indicates that the model is a better fit to the data. This allowed us to identify the best models that explain the mean generalized force profiles. For these best-fit models, we then repeated the fitting to the profiles of each participant. This individual fitting serves as an indication for the variance of the optimal weights fitted to the mean force profile. In addition, to examine the overall fit of the models, we fitted the models to the entire dataset, i.e. all four experiments, followed by a BIC calculation for each model.

Statistical Analysis

To compare the phase differences between the scaled force field curve and the force compensation curves we fitted a one-way repeated measures ANOVA model with phase difference as the dependent factor and the workspace as the within-subject independent factor (3 levels; difference between the training workspace, workspace 1 and workspace 2 and the scaled force field). We repeated this test for all experiments. When the phase factor was found to be statistically significant, we used post-hoc tests with a Bonferroni correction for multiple comparisons. Statistical significance was determined at the 0.05 threshold in all tests.

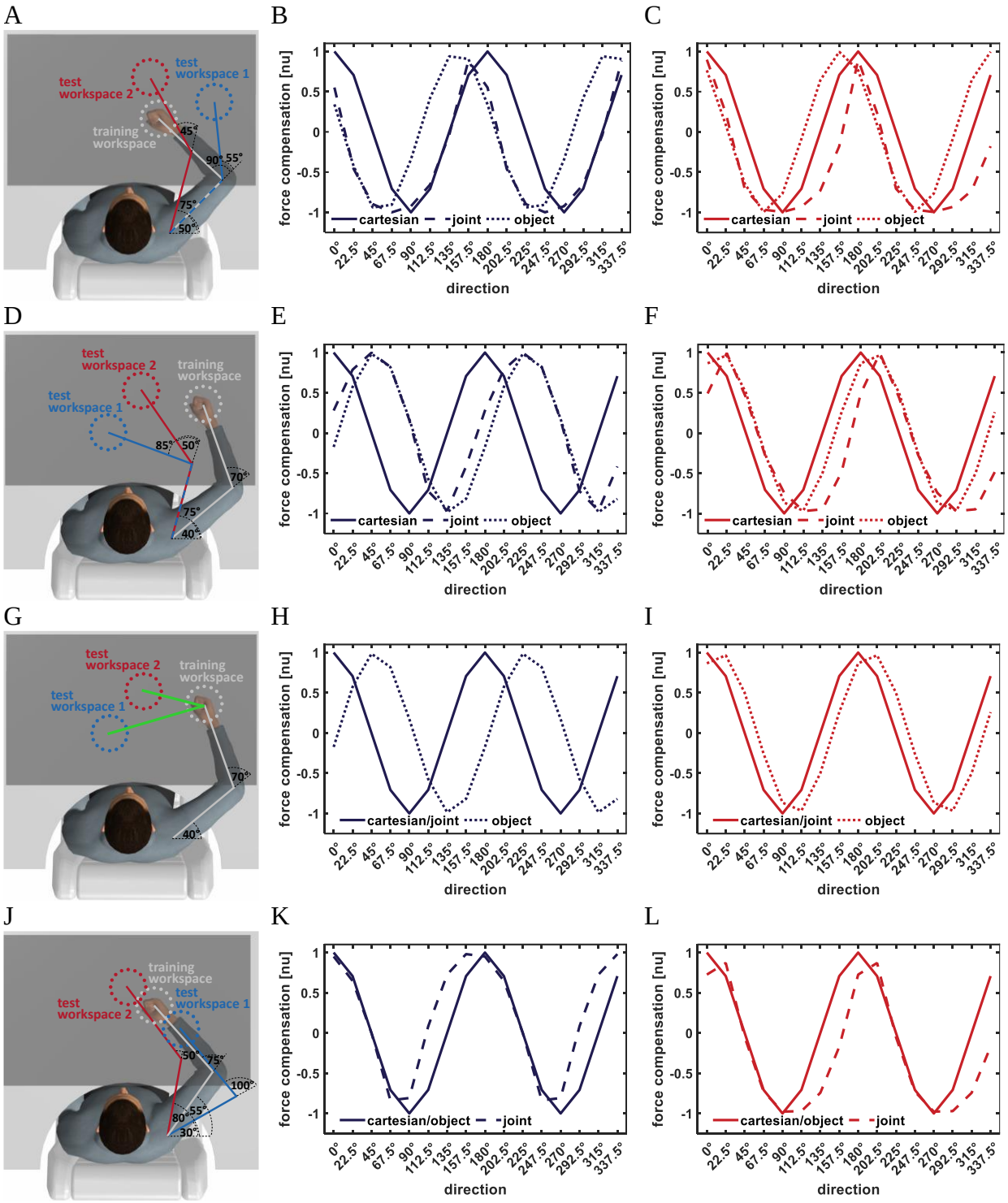

Figure 2: Workspaces locations and force generalization predictions of the models. **A)** Workspaces locations for experiment 1. Participants adapted to the scaled curl force field in the training workspace (grey) while force generalization was tested in test workspace 1 (blue) and test workspace 2 (red). Each workspace location was set based on predefined values of shoulder and elbow joint angles and the measured length of the upper and forearm. Only the start and target locations for the current movement were displayed on each trial. **B)** Force compensation predictions for test workspace 1 in experiment 1 for Cartesian (solid line), joint (dashed line), or object (dotted line) representations of the dynamics. **C)** Force

compensation predictions for test workspace 2 in experiment 1. **D)** Workspaces locations for experiment 2. **E&F)** Force compensation predictions for test workspaces in experiment 2. **G)** Workspace locations for experiment 3. The participants always moved in the training workspace and the generalized forces were measured during movement of the endpoint of a pole (visually attached to the hand) in the same test workspaces as in experiment 1. **H&I)** Force compensation predictions for test workspaces in experiment 3. **J)** Workspace locations for experiment 4. **K&L)** Force compensation predictions for test workspaces in experiment 3.

Across all test workspaces and experimental conditions, the Cartesian based representation predicts the same generalized force pattern as the learned force field. When the arm configuration differs between training and test workspaces, the joint-based representation predicts a shift to the right (panels E, F and L), left (panels B and K) or both (panel C) of the generalized force pattern with respect to the learned force field. When the hand orientation differs between training and test workspaces, the object-based representation predicts a shift to the right (panels E, F, H, and I) or left (panels B and C) of the generalized force pattern.

Results

In experiment 1, participants adapted to the scaled curl force field as indicated by both the reduction in maximum perpendicular error (Figure 3A) and the increase in predictive force compensation profile in the training workspace (Figure 3B, grey curve) that resembles the cosine tuning of the scaled force field (Figure 1D). The generalized force compensation in test workspaces 1 and 2 also exhibited a cosine pattern; however, it was shifted with respect to the curve of the training workspace or the curve representing the force field. For the curve calculated based on movements in the training workspace (Figure 3B and 3C, grey curve) we did not find a shift in respect to the original curve describing the force field (-0.01±0.03°, mean±STD). For the curve calculated based on movements in test workspace 1 (Figure 3B, blue curve), we found a leftward shift of -23±4.8° in respect to the original curve describing the force field. For the curve calculated based on movements in test workspace 2 (Figure 3B, red curve) we again found a leftward shift of the curve, however, this shift (-6.3±4.8°) was smaller compared with the shift we found for test workspace 1. These observations were confirmed using a repeated measures ANOVA that showed a statistically significant effect of the workspace condition ($F_{2,14}$=115.6, p<0.001). Post-hoc analysis showed that the training curve was not statistically significantly different from the force field curve (t_7=1, p=0.35). However, both curves for workspace 1 and workspace 2 were statistically significant different from the force field curve (both t_7>3.7, p<0.01), from the training workspace curve (both t_7>3.72, p<0.05) and from each other (t_7=13.4, p<0.001).

These trends match the trends predicted by a mixture model that rely mostly on the object-based representation. The object-based representation predicts a leftward shift of the curve based on test workspace 1 (Figure 3C upper panel, dot curve) and a smaller leftward shift of the curve based on test workspace 2 (Figure 3C bottom panel, dot curve). Importantly, for some of the directions, only the simulation based on the object-based representation predicted the leftward shift we observed for the curve of workspace 1 and 2. When fitted to the data, we found that a mixture model combining the Cartesian, joint- and object-based representation (C+J+O) with a decay factor best fits the experimental results (Figure 3D). The optimal weights of this model were 0.31 for the contribution of the object-based representation and 0.22 and 0.1 for the contribution of the joint-based and Cartesian based representations respectively. Another mixture model that fits the data was a mixture of the object- and joint- based representations (J+O) with a decay factor. For this

model we found that the object-based representation had a weight 0.33 and the joint-based representation had a weight of 0.28.

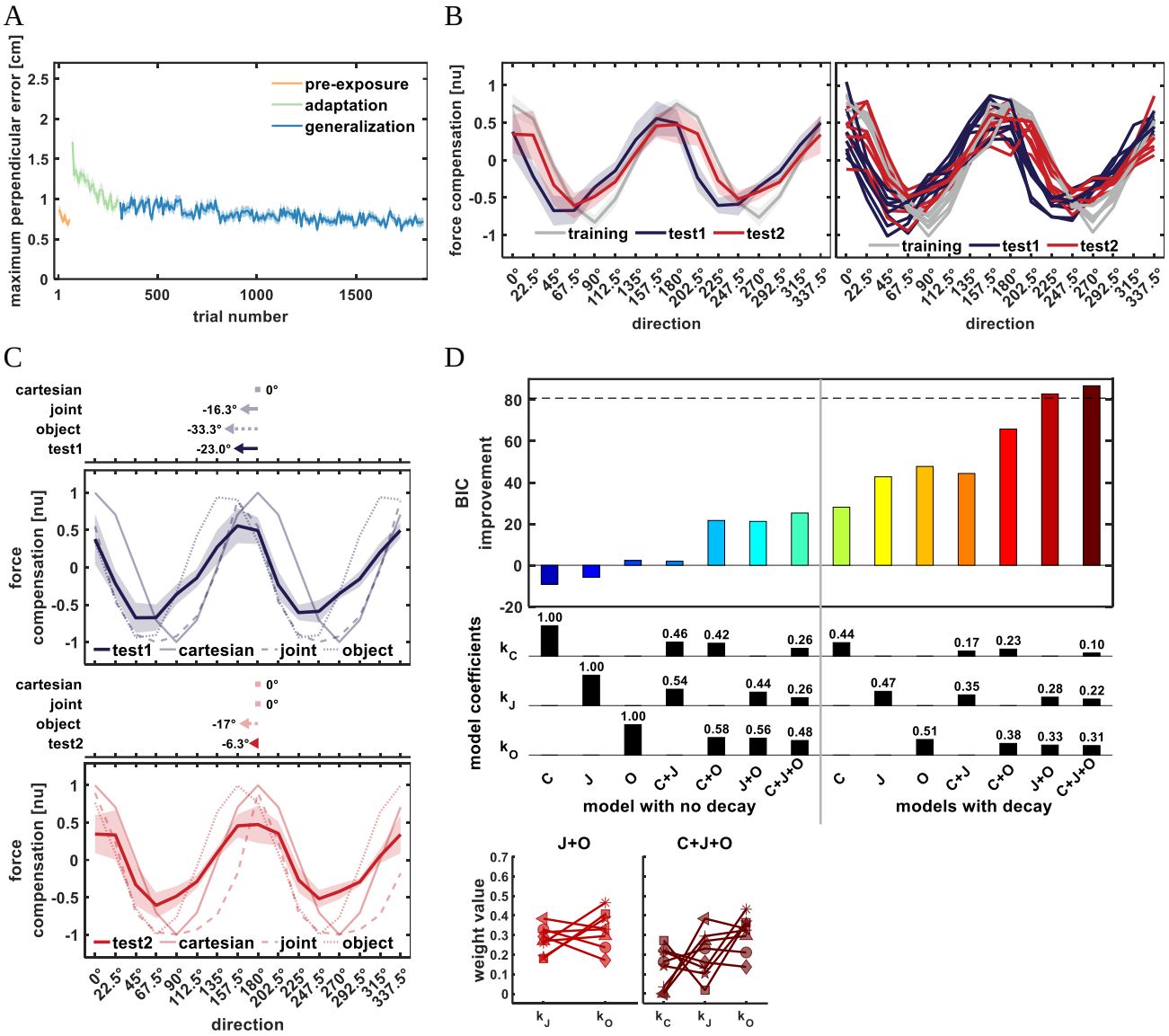

Figure 3: Results of experiment 1.

A) Mean maximum perpendicular error (MPE) and standard error (shaded area) across participants during pre-exposure phase (orange line), adaptation phase (green line), and generalization phase (blue line) of movements performed in the training workspace.

B) Left panel, mean force compensation profiles. Participants were able to adapt to the scaled force field as evident by the force compensation profile in the training workspace (grey curve) and showed a rightward shift of the curve for the test workspace 2 (red curve) and more so for test workspace 1 (blue curve). Right panel, Individual force compensation profiles for each participant in the training workspace (grey curve), workspace 1 (blue curve), and workspace 2 (red curve).

C) Upper panel, mean force compensation profile for workspace 1 (dark blue solid line) and Cartesian (light blue solid line), joint- (light blue dashed line), and object- (light blue dotted line) based model predictions (same as Fig. 2B). Bottom panel, mean force compensation profile for workspace 2 (dark red solid line) and

Cartesian (light red solid line), joint- (light red dashed line), and object- (light red dotted line) based model predictions (same as Fig. 2C). Arrows at the top of the panels indicate the shift of the mean force compensation profile and the models predictions in respect to the original curve describing the force field.
D) Upper panel, BIC Improvement for each of the models relative to no generalization (that is, a model in which the force is zero at all movement directions). Dashed line shows the cutoff for models that are not considered distinguishable in terms of their performance from the best model (C+J+O model). Middle panel, the fitted coefficients for each model. C- Cartesian, J- joint, O- object. Bottom panels are the fitted coefficients for the best models (J+O and C+J+O) when fitting the models to individual participant data, indicating the variance of the fitted coefficients values.

In experiment 2, we found similar adaption trend to the scaled curl force field as seen in the reduction in maximum perpendicular error (Figure 4A). The force compensation curve in the training workspace resembles the cosine tuning of the scaled force field (Figure 4B, grey curve), and we found similar pattern for the force compensation in test workspaces 1 and 2 but for this experiment they were shifted to the right with respect to the curve of the training workspace or the curve representing the force field. Similar to experiment 1, the curve calculated based on movements in the training workspace was not shifted in respect to the original curve describing the force field (-1±2.45°, mean±STD). For the curve calculated based on movements in test workspace 1 (Figure 3B, blue curve), we found a rightward shift of 34.5±1.2° in respect to the original curve describing the force field. For the curve calculated based on movements in test workspace 2 (Figure 3B, red curve) we again found a significant rightward shift of the curve, however, this shift of 15.4±4.4° was smaller compared with the shift we found for test workspace 1. These observations were confirmed using a repeated measures ANOVA that showed a statistically significant effect of the workspace condition ($F_{2,14}$=306.8, p<0.001). Post-hoc analysis showed that the training curve was not statistically significantly different from the force field curve (t_7=1.1, p=0.3). However, both curves for workspace 1 and workspace 2 were statistically significantly shifted from the force field curve (both t_7>9.8, p<0.001), from the training workspace curve (both t_7>9.4, p<0.001) and from each other (t_7=12.5, p<0.001).

These trends match the predictions of the joint- and object-based representations. Both representations predicted a rightward shift of the curve based on test workspace 1 (Figure 4C upper panel) and a smaller rightward shift of the curve based on test workspace 2 (Figure 4C bottom panel). When fitted to the data, we found that a mixture model of all three representations (C+J+O) with a decay factor best fits the experimental results (Figure 4D). The optimal weights of the Cartesian, joint- and object-based representations were 0.14, 0.28, and 0.28 respectively. Another

mixture model that fits the data was a mixture of the Cartesian (optimal weight, 0.16) and the object-based representation (optimal weight, 0.53) with a decay factor.

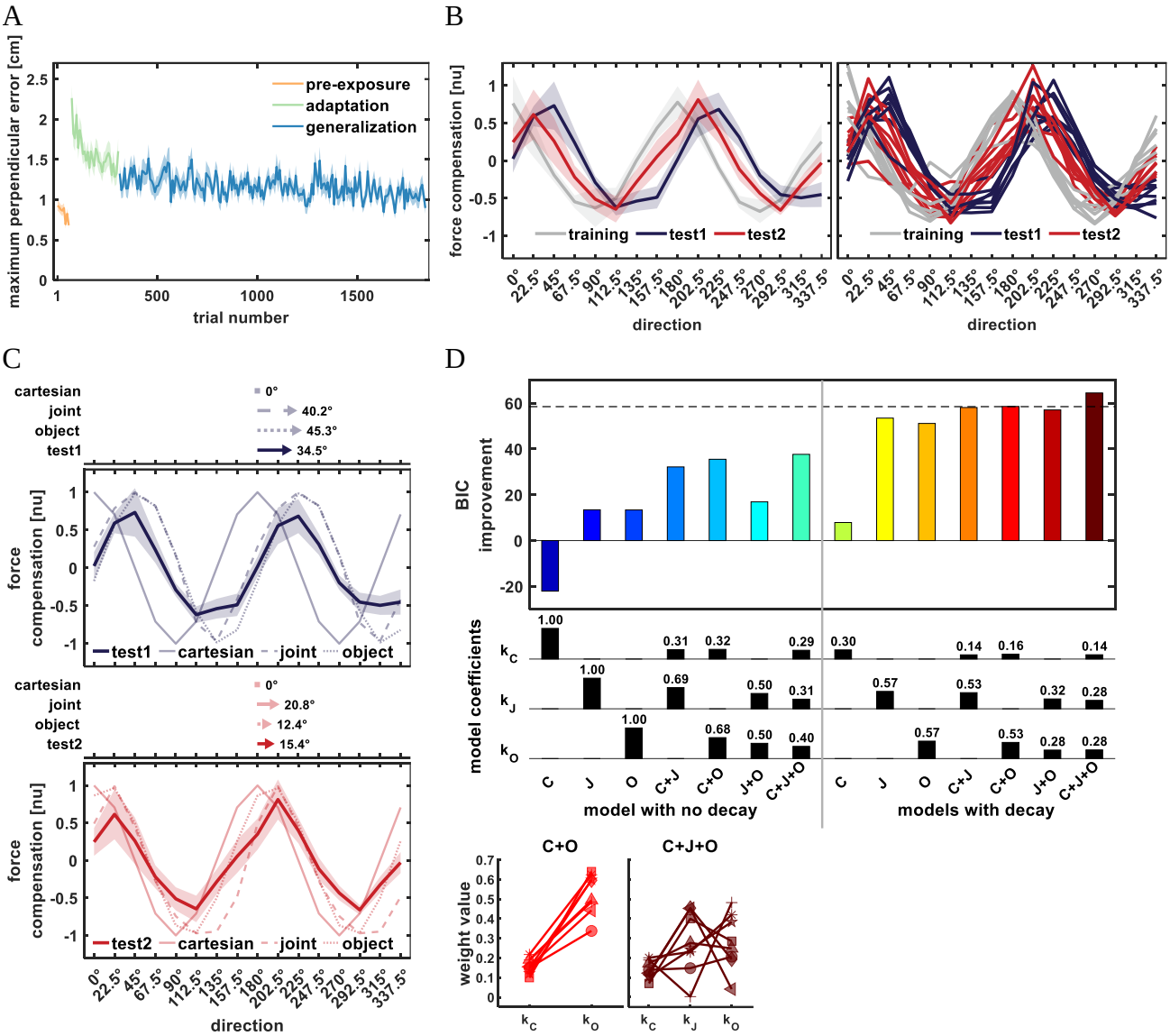

Figure 4: Results of experiment 2. All notations are similar to Figure 3.

A) Mean maximum perpendicular error (MPE).

B) Left panel, mean force compensation profiles in the training and test workspaces. Right panel, individual force compensation profiles in the training and test workspaces.

C) Upper panel, mean force compensation profile for workspace 1 and model predictions (same as Fig. 2E). Bottom panel, mean force compensation profile for workspace 2 and model predictions (same as Fig. 2F). Arrows at the top of the panels indicate the shift of the mean force compensation profile and the models predictions in respect to the original curve describing the force field.

D) Upper panel, BIC Improvement for each of the models relative to no generalization. Dashed line shows the cutoff for models that are not considered distinguishable in terms of their performance from the best model (C+J+O model). Middle panel, the fitted coefficients for each model. C- Cartesian, J- joint, O- object. Bottom panels are the fitted coefficients for the best models (C+O and C+J+O) when fitting the models to individual participant data.

In experiment 3, after adaptation to the scaled force field in the training workspace (Figure 5A), participants had to move the tip of a pole between start and target positions in the test workspaces. That is, the arm posture did not change between the adaptation and generalization parts of the experiment. In this case, both the Cartesian and joint-based representations predict that the force compensation curve for the test workspaces will not shift compared with the force compensation curve for the training workspace. Contrary to these predictions, the object-based representation predicts a rightward shift for both workspace 1 and 2, with a stronger shift for workspace 1 (Figure 2H and 2I, dotted curves). We found a rightward shift of the curve for both test workspaces with respect to the training workspace. For the curve calculated based on movements in the training workspace (Figure 5B, grey curve) we did not find a shift with respect to the original curve describing the force field (-0.05±0.14°, mean±STD). For the curve calculated based on movements in test workspace 1, we found a rightward shift of 17±5.7° (Figure 5B, blue curve). For the curve calculated based on movements in test workspace 2 we again found a rightward shift of the curve, however, this shift (4.5±3.6°) was smaller compared with the shift we found for test workspace 1 (Figure 5B, red curve). These observations were confirmed using a repeated measures ANOVA that showed a statistically significant effect of the workspace condition ($F_{2,14}$=66.0, p<0.001). Post-hoc analysis showed that the training curve was not statistically significantly different from the force field curve (t_7=1, *p*=0.351). For test workspaces 1 and 2, we found a statistically significant shift of the force compensation curves of these workspaces from the force field curve (both t_7>3.5, p<0.05), from the training workspace force compensation curve (both t_7>3.6, p<0.05), and from each other (t_7=9.96, *p*<0.001).

Similar to the results of experiment 2, we found that the object-based model predicts the rightward shifts of the force compensation curves of test workspaces 1 and 2 (Figure 5C). The best model that capture these results is a mixture model combining the Cartesian or joint-based representations with the object-based representation (C+O or J+O) with a decay factor (Figure 5D). The optimal weights of these models were 0.24 for the contribution of the object-based representation and 0.39 for the contribution of the Cartesian or joint-based representations. Since the Cartesian and joint-based representations predict the same generalized forces curves we cannot distinguish between them, however, the best fit to the experimental data is a result of combining either of these representations with the object-based representation. Other models that can explain the data were Cartesian based model (C), joint-based model (J), and a mixture of all three representations

(C+J+O). This last mixture model had same weight value (0.24) for the object-based representation as in the C+O or J+O models and an equally divided weight for the Cartesian and joint-based representation (0.195) since these two representations predicted similar curves for this experiment. The individual Cartesian or joint-based models were also not distinguishable from the best model since the rightward shifts were not as strong as in experiment 2.

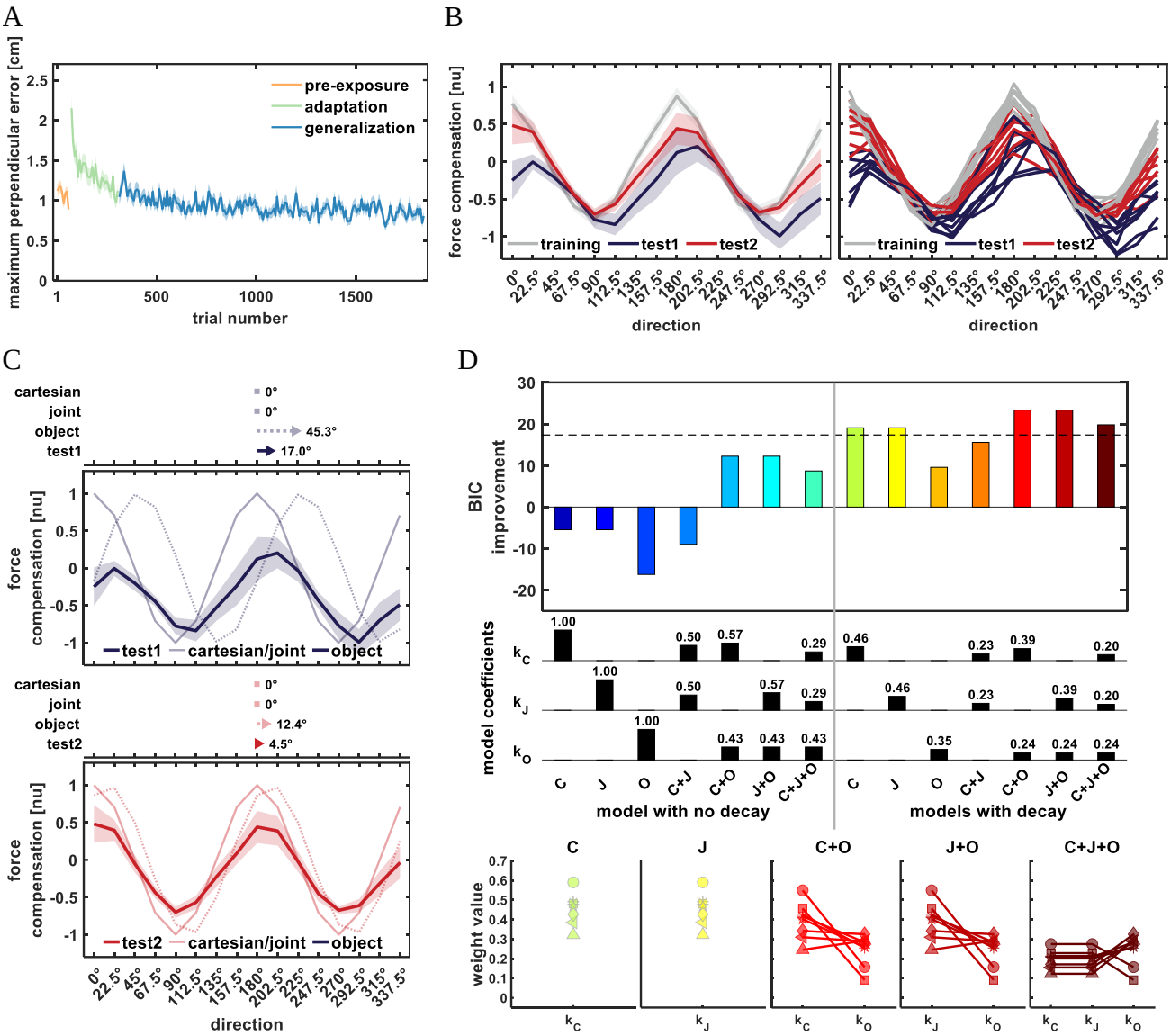

Figure 5: Results of experiment 3. All notations are similar to Figure 3.

A) Mean maximum perpendicular error (MPE).

B) Left panel, mean force compensation profiles in the training and test workspaces. Right panel, individual force compensation profiles in the training and test workspaces.

C) Upper panel, mean force compensation profile for workspace 1 and model predictions (same as Fig. 2H). Bottom panel, mean force compensation profile for workspace 2 and model predictions (same as Fig. 2I). Arrows at the top of the panels indicate the shift of the mean force compensation profile and the models predictions in respect to the original curve describing the force field.

D) Upper panel, BIC Improvement for each of the models relative to no generalization. Dashed line shows the cutoff for models that are not considered distinguishable in terms of their performance from the best model (C+O or J+O models). Middle panel, the fitted coefficients for each model. C- Cartesian, J- joint, O- object. Bottom panels are the fitted coefficients for the best models (C, J, C+O, J+O, and C+J+O) when fitting the models to individual participant data.

In experiment 4, we found similar adaptation to the scaled force field as evident by the reduction in MPE (Figure 6A). In this experiment, we set the location of the training and test workspaces in such way that the hand orientation did not change across workspaces. In this case, both the Cartesian and object-based representations predict that the curves extracted from movements in the test workspaces will resemble the one extracted from the training workspace. Contrary to these predictions, the joint-based representation predicts a leftward shift for the force compensation curve extracted from test workspaces 1 and a rightward shift for the curve extracted from test workspaces 2. For the curve calculated based on movements in the training workspace (Figure 6B, grey curve) we did not find significant shift in respect to the original curve describing the force field (-0.03±0.07°, mean±STD). For test workspace 1, we found a small leftward shift of -3.7±3.1° (Figures 6B, 6C blue curve) and for test workspace 2 we found a rightward shift of 6.8±1.8 ° (Figures 6B, 6C red curve). These observations were confirmed using a repeated measures ANOVA that showed a statistical significant effect of the workspace condition (Greenhouse-Geisser correction $F_{1.11,7.83}=41.6$, $p<0.001$). Post-hoc analysis showed that the training curve was not statistically significantly different from the force field curve ($t_7=1$, $p=0.35$). For both test workspace 1 and 2, we found statistically significant difference between the force compensation curve and both the force field curve (both $t_7=3.36$, $p<0.05$) and the training workspace force compensation curve (both $t_7=3.31$, $p<0.05$). We also found significant difference between the force compensation curves of workspace 1 and 2 ($t_7=6.6$, $p=0.001$).

Using the BIC analysis (Figure 6D), we found that the best models to explain the results were mixture models combining the Cartesian or object-based representation with the joint-based representation (C+J or J+O). The optimal weights of these models were 0.31 for the contribution of the joint-based representation and 0.35 for the contribution of the Cartesian or object-based representations. Another model that can explain the data was a mixture of all three representations (C+J+O). This last mixture model had same weight value (0.31) for the joint-based representation as in the C+J or J+O models and an equally divided weight for the Cartesian and object-based representation (0.175) since these two representations predicted similar curves for this experiment.

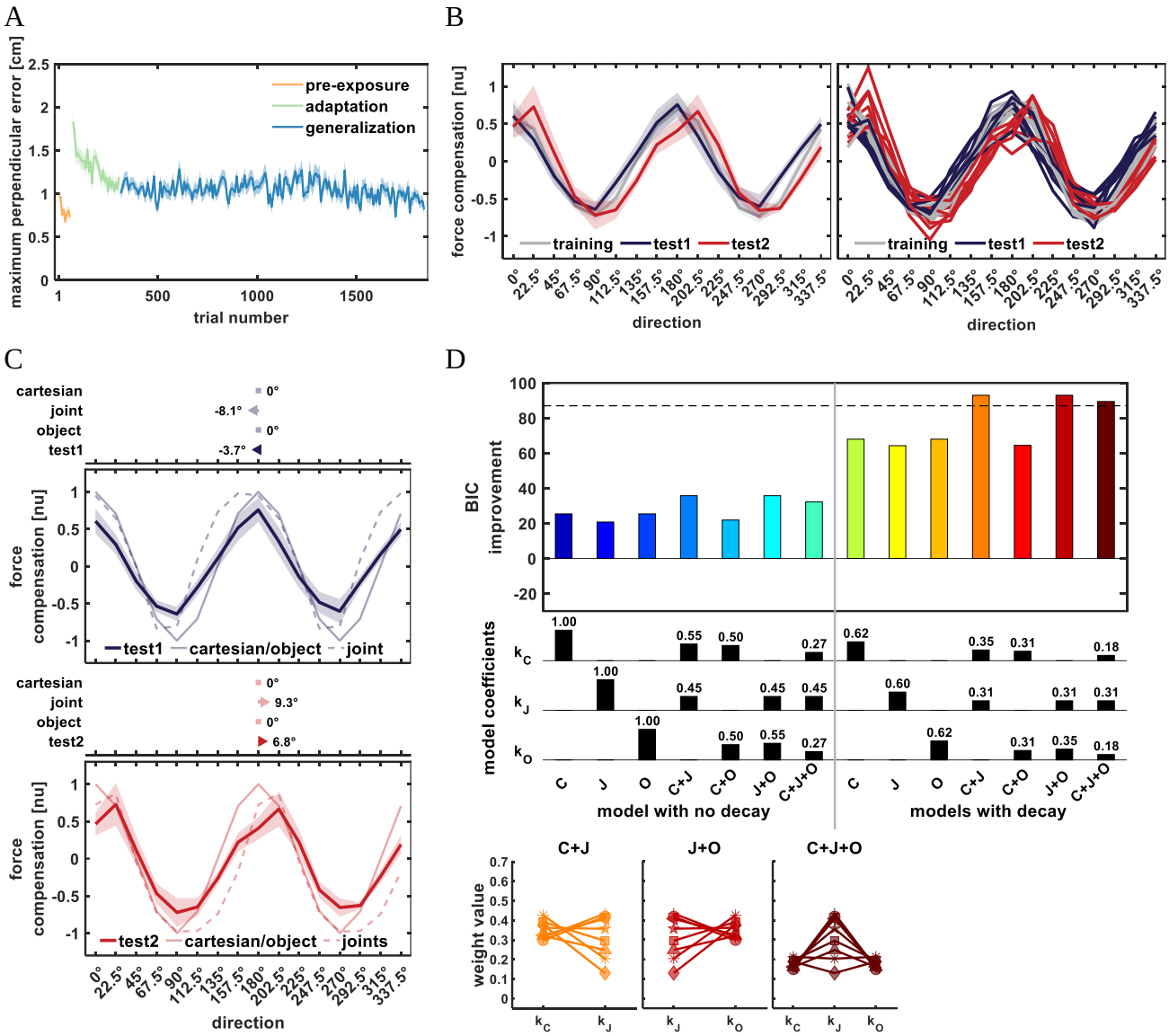

Figure 6: Results of experiment 4. All notations are similar to Figure 3.

A) Mean maximum perpendicular error (MPE).

B) Left panel, mean force compensation profiles in the training and test workspaces. Right panel, individual force compensation profiles in the training and test workspaces.

C) Upper panel, mean force compensation profile for workspace 1 and model predictions (same as Fig. 2K). Bottom panel, mean force compensation profile for workspace 2 and model predictions (same as Fig. 2L). Arrows at the top of the panels indicate the shift of the mean force compensation profile and the models predictions in respect to the original curve describing the force field.

D) Upper panel, BIC Improvement for each of the models relative to no generalization. Dashed line shows the cutoff for models that are not considered distinguishable in terms of their performance from the best model (C+J or J+O models). Middle panel, the fitted coefficients for each model. C- Cartesian, J- joint, O- object. Bottom panels are the fitted coefficients for the best models (C+J, J+O, and C+J+O) when fitting the models to individual participant data.

The mixed model of Cartesian, joint- and object-based representation was the only model that explained the data across all four experiments. To further analyze the coordinate representation across all experiments, we fitted the models to the data of the four experiments combined. We found that the best model was a mixed model of Cartesian, joint- and object-based representation scaled by the decay factor (Figure 7). The weights for the Cartesian, joint- and object-based representation were 0.11, 0.267 and 0.271 respectively. Moreover, only this model was selected as one of the best-fitting models across all four experiments. This suggests that representation of ambiguous external dynamics is formed by a mixture of Cartesian, joint- and object-based coordinate systems.

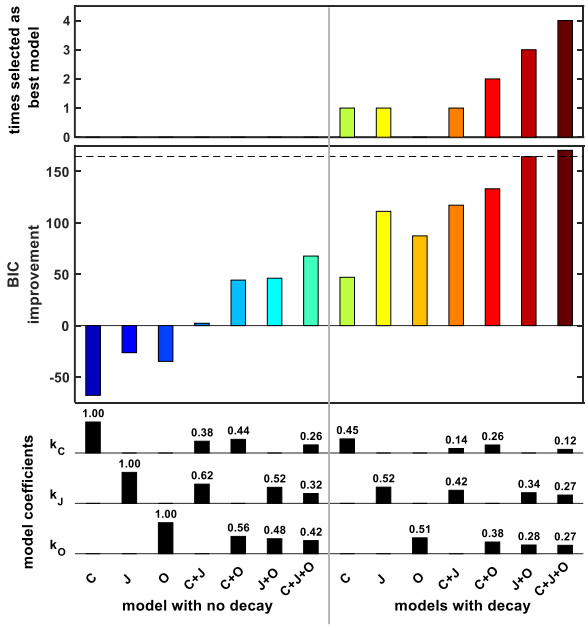

Figure 7: Upper panel shows the number of experiments that each model was able to explain when fitted to the data of each of the four experiments. Only one model (C+J+O) was selected for all four experiments. Middle panel is BIC improvement for each of the models fitted to all four experiments relative to no generalization. Dashed line shows the cutoff for models that are not considered distinguishable in terms of their performance from the best model (C+J+O model). All other models were below this line. Bottom panel, the fitted coefficients for each model. C- Cartesian, J- joint, O- object.

Discussion

In this study, we examined which coordinate frame the motor system uses during adaptation to novel dynamics. To do so, we analyzed the pattern of generalized forces outside the training workspace where participants adapted to a scaled curl force field. The trigonometric scaling of the force field allowed to easily distinguish which of the three tested representations, i.e. Cartesian, joint-, and object- based representations, was used to represent the external forces. We found that the generalized forces resemble the prediction of a mixture model combining Cartesian, joint- and object-based representations. Importantly, we show that a single reference frame could not explain the generalized forces while a mixture of the models incorporating the object-based representation with increased weight could explain the results. This is opposed to previous findings which considered the three coordinate frames and different combinations of them but could not conclude that the predictions of mixture models are superior to those of single coordinate frame based models (Berniker et al., 2014).

The trigonometric scaling of the curl force field allowed us to distinguish between the Cartesian, joint-, or object-based representations. The perpendicular forces applied on the hand during movement could have different amplitude as well as different direction, i.e. clockwise or counter clockwise direction, as a function of movement direction. Since the forces were perpendicular to movement direction we avoided the issue of assistive or resistive forces during motion while being able to capture the generalized forces using a force channel (Berniker et al., 2014). Along with eliminating factors that might distort the true nature of generalized forces, the trigonometric pattern of forces allowed to test models predictions by examining the phase change between adapted force profile and the generalized force profile. Thus, for each experiment we choose the training and testing workspaces locations so to maximize the phase difference between models predictions.

Initially, we tested generalization where both the posture of the arm and the orientation of the hand changed between training and test locations. In such case, both the joint- and object-based representations predicted a shift of the generalized forces pattern compared with the adapted force pattern while the Cartesian based representation did not predict any phase shift. The shifts of the curves for both test workspaces for experiment 1 and 2, as exhibited by the participants, suggest that the object-based representation was slightly more dominant in representing the external forces.

This result support the idea that the motor system uses this type of coordinate system as suggested by previous studies (Ahmed et al., 2008; Yeo et al., 2015; Franklin et al., 2016).

The idea of the object-based representation suggests that the motor system relates the external forces to a hand-held object, which may be a real object or not, and thus these forces should rotate as the object rotates. Indeed, we observed that the generalized forces in experiment 3 rotated with the rotation of the hand-held object. We observed that the expected forces were a result of combining the object-based representation with either the Cartesian or joint-based representation. This is in-line with previous studies which suggested that during object manipulation the motor system relies on such combination of reference frames (Ahmed et al., 2008). However, other studies suggested that dynamics during object manipulation are represented in joint-based coordinate frame (Mah and Mussa-Ivaldi, 2003; Bays and Wolpert, 2006). As suggested by Ahmed et al. (2008), a possible explanation for discrepancy might be that the motor system can gradually switch between coordinate frames and this might be affected by the visual information about the object or familiarity with it. The results reported here fit with this explanation since we provided full visual feedback about the pole, which might trigger such transitions between coordinate frames. Thus, we suggest that the greater weight of the Cartesian or joint- based representation compared with the weight for the object-based representation (0.39 vs. 0.24) to the overall generalization forces might be a result of an incomplete transition process. Extensive training over days may change this ratio in favor of the object-based representation and remains an open question for future studies.

Another way to test the contribution of the object-based representation for dynamics representation is by examining force generalization with the same hand orientation. In such case, changing joints angles, and thus the arm configuration, will not change the generalized forces pattern compared with the learned forces pattern. Indeed, we found small phase deviations of the force compensation curves between the training and test workspaces despite the spatial difference between them. The predictions of the joint-based representation were consistent with the small phase deviations we found in shift direction but not in the shift magnitude. This was also confirmed by the fitting of the mixture models that had increased weight for the Cartesian or object-based representation compared with weight for the joint-based representation. Thus, these results suggest that the

relative contribution of the joint-based representation is slightly lower than the contribution of the object-based representation.

Whether there is evidence for neural encoding of an object-based representation is still an open question. Given that this representation was not considered in early studies, the interpretation of neural activity mostly focused on Cartesian and joint-based representations. For example, there is evidence that during isometric force generation task the activity on the primary motor cortex (M1) is represented in intrinsic, joint-based coordinate frame (Sergio and Kalaska, 2003). This was also evident examining generalization of novel dynamics for children with autism spectrum disorder (Haswell et al., 2009). However, since most efforts understating the neural basis of coordinate representation focused on examining movement planning and execution, the neural representation of forces is yet to be established.

We expect that these representations might be stored in areas related to forward and inverse models. During motor adaptation, the sensorimotor system might change both the controller (inverse model) and the predictor (forward model) to modify the control so as to overcome changes in the environment (Flanagan et al., 2003; Franklin et al., 2008). The cerebellum has been proposed to host both types of internal models (Wolpert and Kawato, 1998; Smith and Shadmehr, 2005), however, other areas might also be involved during adaption to altered environment dynamics. For example, changes in premotor cortex (PMd) activity were also evident during force field adaptation (Perich et al., 2018). Generalization of the learned dynamics to different locations in space might require from both the inverse and forward model to use dynamics transformation such as the ones considered in this study. Thus, we speculate that such transformation might be evident in the neural activity of these areas during adaptation to novel dynamics.

The results we present here support the idea that the motor system can use multiple representations during adaptation to novel dynamics. However, based on these results we cannot determine the trigger for favoring one coordinate frame over another. Since the force field is ambiguous (i.e. the force field appeared in a small workspace with no constraints on which coordinate frame to use for representation of the dynamics) it can be represented in any of the suggested coordinate frames including a mixture of them. Using unambiguous force fields that extend over larger area of the workspace according to one coordinate frame (Franklin et al., 2016) might result in using a single coordinate frame for dynamics representation.

Force generalization has been an important way to test the coordinate system the motor system uses to represent information (Franklin and Wolpert, 2011). The initial idea that the motor system uses intrinsic, joint-based representation (Shadmehr and Mussa-Ivaldi, 1994) is more questionable nowadays as more evidence accumulated showing that the motor system can use and switch between other coordinates systems (Ahmed et al., 2008; Berniker et al., 2014; Saha et al., 2015). We show additional evidence that the motor system uses a mixture of models (Brayanov et al., 2012; Berniker et al., 2014) with slightly increased weight for the object-based representation. Using a force field which overcomes some of the weaknesses other force fields have, we were able to support this fairly new idea of mixture models which include an object-based representation. This type of force field can be used for other types of generalization tests, such as inter-limb transfer (Criscimagna-Hemminger et al., 2003) or characterizing brain related disorders (Haswell et al., 2009), to reveal more characteristics of the information representation.

References

Ahmed AA, Wolpert DM, Flanagan JR (2008) Flexible Representations of Dynamics Are Used in Object Manipulation. Current Biology 18:763-768.

Bays PM, Wolpert DM (2006) Actions and Consequences in Bimanual Interaction Are Represented in Different Coordinate Systems. The Journal of Neuroscience 26:7121-7126.

Berniker M, Franklin DW, Flanagan JR, Wolpert DM, Kording K (2014) Motor learning of novel dynamics is not represented in a single global coordinate system: evaluation of mixed coordinate representations and local learning. Journal of Neurophysiology 111:1165-1182.

Brayanov JB, Press DZ, Smith MA (2012) Motor Memory Is Encoded as a Gain-Field Combination of Intrinsic and Extrinsic Action Representations. The Journal of Neuroscience 32:14951-14965.

Criscimagna-Hemminger SE, Donchin O, Gazzaniga MS, Shadmehr R (2003) Learned Dynamics of Reaching Movements Generalize From Dominant to Nondominant Arm. Journal of Neurophysiology 89:168-176.

Flanagan JR, Vetter P, Johansson RS, Wolpert DM (2003) Prediction Precedes Control in Motor Learning. Current Biology 13:146-150.

Franklin David W, Wolpert Daniel M (2011) Computational Mechanisms of Sensorimotor Control. Neuron 72:425-442.

Franklin DW, Batchelor AV, Wolpert DM (2016) The Sensorimotor System Can Sculpt Behaviorally Relevant Representations for Motor Learning. eneuro 3:ENEURO.0070-0016.2016.

Franklin DW, Burdet E, Peng Tee K, Osu R, Chew C-M, Milner TE, Kawato M (2008) CNS Learns Stable, Accurate, and Efficient Movements Using a Simple Algorithm. The Journal of Neuroscience 28:11165-11173.

Gandolfo F, Mussa-Ivaldi FA, Bizzi E (1996) Motor learning by field approximation. Proceedings of the National Academy of Sciences 93:3843-3846.

Haswell CC, Izawa J, Dowell LR, Mostofsky SH, Shadmehr R (2009) Representation of internal models of action in the autistic brain. Nature neuroscience 12:970-972.

Howard IS, Ingram JN, Wolpert DM (2009) A modular planar robotic manipulandum with end-point torque control. Journal of Neuroscience Methods 181:199-211.

Mah CD, Mussa-Ivaldi FA (2003) Generalization of Object Manipulation Skills Learned without Limb Motion. The Journal of Neuroscience 23:4821-4825.

Malfait N, Shiller DM, Ostry DJ (2002) Transfer of Motor Learning across Arm Configurations. The Journal of Neuroscience 22:9656-9660.

Milner TE, Franklin DW (2005) Impedance control and internal model use during the initial stage of adaptation to novel dynamics in humans. The Journal of Physiology 567:651-664.

Oldfield RC (1971) The assessment and analysis of handedness: The Edinburgh inventory. Neuropsychologia 9:97-113.

Parmar PN, Huang FC, Patton JL (2011) Simultaneous coordinate representations are influenced by visual feedback in a motor learning task. In: 2011 Annual International Conference of the IEEE Engineering in Medicine and Biology Society, pp 6762-6768.

Perich MG, Gallego JA, Miller LE (2018) A Neural Population Mechanism for Rapid Learning. Neuron 100:964-976.e967.

Saha DJ, Hu X, Perreault E, Murray W, Mussa-Ivaldi FA (2015) The coordinate system for force control. Experimental Brain Research 233:899-908.

Scheidt RA, Dingwell JB, Mussa-Ivaldi FA (2001) Learning to Move Amid Uncertainty. Journal of Neurophysiology 86:971-985.

Sergio LE, Kalaska JF (2003) Systematic Changes in Motor Cortex Cell Activity With Arm Posture During Directional Isometric Force Generation. Journal of Neurophysiology 89:212-228.

Shadmehr R, Mussa-Ivaldi F (1994) Adaptive representation of dynamics during learning of a motor task. The Journal of Neuroscience 14:3208-3224.

Smith MA, Shadmehr R (2005) Intact Ability to Learn Internal Models of Arm Dynamics in Huntington's Disease But Not Cerebellar Degeneration. Journal of Neurophysiology 93:2809-2821.

Smith MA, Ghazizadeh A, Shadmehr R (2006) Interacting Adaptive Processes with Different Timescales Underlie Short-Term Motor Learning. PLOS Biology 4:e179.

Wolpert DM, Kawato M (1998) Multiple paired forward and inverse models for motor control. Neural Networks 11:1317-1329.

Yeo S-H, Wolpert DM, Franklin DW (2015) Coordinate Representations for Interference Reduction in Motor Learning. PLoS One 10:e0129388-e0129388.